

Closed-Loop Molecular Communication with Local and Global Degradation: Modeling and ISI Analysis

Lukas Brand, Fardad Vakilipoor, Sören Botsch, Timo Jakumeit, Sebastian Lotter, Robert Schober, and Maximilian Schäfer

Friedrich-Alexander-Universität Erlangen-Nürnberg, Erlangen, Germany

ABSTRACT

This paper presents a novel physics-based model for signal propagation in closed-loop molecular communication (MC) systems, which are particularly relevant for many envisioned biomedical applications, such as health monitoring or drug delivery within the closed-loop human cardiovascular system (CVS). Compared to open-loop systems, which are mostly considered in MC, closed-loop systems exhibit different characteristic effects influencing signaling molecule (SM) propagation. One key phenomenon are the periodic SM arrivals at the receiver (RX), leading to various types of inter-symbol interference (ISI) inherent to closed-loop system. To capture these characteristic effects, we propose an analytical model for the SM propagation inside closed-loop systems. The model accounts for arbitrary spatio-temporal SM release patterns at the transmitter (TX), and incorporates several environmental effects such as fluid flow, SM diffusion, and SM degradation. Moreover, to capture a wide range of practically relevant degradation and clearance mechanisms, the model includes both local removal (e.g., due to SM absorption into organs) and global removal (e.g., due to chemical degradation) of SMs. The accuracy of the proposed model is validated with three-dimensional (3-D) particle-based simulations (PBSs). Moreover, we utilize the proposed model to develop a rigorous characterization of the various types of ISI encountered in closed-loop MC systems.

CCS CONCEPTS

• **Applied computing** → *Mathematics and statistics*; • **Computing methodologies** → **Model development and analysis**; *Molecular simulation*.

KEYWORDS

Molecular Communication (MC), Closed-Loop Systems, MC System Modeling, IoBNT, Signal Propagation, Advection-Diffusion Model, Inter-Symbol Interference (ISI), Partial Differential Equation (PDE)

1 INTRODUCTION

Molecular communication (MC) is a growing research field at the intersection of life sciences and engineering. One main direction of MC research lies in the medical sector, aiming at the development of innovative diagnosis and therapeutic strategies for future healthcare systems, focusing on applications such as early disease detection or targeted treatment [1, 5]. In early disease detection, chemical signals that are potentially indicative of diseases, are sensed and processed inside the human body by synthetic nanodevices such as synthetic cells or nanorobots [2]. In other future applications of MC, in-body devices are envisioned to be equipped with capabilities to transmit, receive, and process molecular signals

in order to communicate with biological entities or with each other to coordinate their actions during disease treatment.

In most disease detection applications, the MC signal is a *natural signal*, i.e., it emanates from a natural biological transmitter (TX), e.g., diseased tissue, and nanodevices act as receivers (RXs). For communicating nanodevices, the MC signal is a *synthetic signal*, i.e., engineered nanodevices act as TXs and RXs. Irrespective of the signal's origin, in both cases, signal propagation from the TX to the RX takes place inside the human body, mostly along the cardiovascular system (CVS) [10]. Hence, it is of vital importance for medical applications of MC to understand the characteristics of molecular signal propagation inside the CVS.

Many studies in MC consider the flow-based transport of molecules in cylindrical geometries as an approximation for molecular signal propagation in the CVS. Most earlier works focus on the development of basic models [5, 12, 15, 20], where molecule transport in a *single blood vessel* is commonly modeled as advection-diffusion process, and *vessel networks* are modeled as equivalent electrical networks [5, 7, 8]. Besides these theoretical works, also a growing number of experimental studies explore flow-dominated MC in cylindrical structures (tubes), see [11] for a recent review. However, most of the existing theoretical and experimental studies consider *open-loop* systems, i.e., there exist perfect *sources* and *sinks* for the carrier medium (and, hence, also for the signaling molecules (SMs)). Consequently, the communication-theoretical tools, e.g., inter-symbol interference (ISI) mitigation strategies, developed in these studies, have been validated only for open-loop MC systems¹.

In contrast, in practical application environments of in-body MC systems, the carrier medium, i.e., blood, is circulating in a closed-loop inside the CVS. This indicates a systematic gap between most MC systems investigated so far, and the envisioned CVS-based real-world MC systems. Some recent experimental studies have considered closed-loop MC systems [4, 14, 17], accumulating evidence that closed-loop systems exhibit characteristic properties, which necessitate specifically tailored communication system designs. In particular, novel types of interference were identified experimentally in [4] that may occur in closed-loop systems but not in open-loop systems. However, while a first phenomenological model for particle distribution in closed-loop systems has been proposed in [14], these recent findings have not been complemented yet by a comprehensive theory for signal propagation in closed-loop MC systems. For example, the model in [14] does not reveal the impact of physical system parameters such as vessel diameters on SM propagation, and it does not account for the impact of molecule

¹Ref. [7] is an exception here, since it considers a closed-loop system. However, a steady-state molecule distribution is assumed for the analysis in [7], limiting its applicability to communication system design.

degradation. Such molecule degradation effects are crucial to consider, as they may arise either naturally in the CVS, e.g., from the clearance of SMs by organs such as the liver or the kidneys, or in experimental systems because of the intentional (partial) removal or inactivation of SMs [16]. In summary, theoretical tools for the analysis and design of closed-loop MC systems do currently not exist. In this paper, we aim to lay the foundation for closing this research gap. In particular, we make the following contributions:

- We propose a physics-based model for flow-based closed-loop MC systems, along with a novel closed-form analytical expression for the SM concentration. The proposed model accounts for the impact of diffusion and flow on the SMs propagating in closed-loop systems. Moreover, it allows for arbitrary release profiles, and incorporates the influence of various biological (e.g., clearance by organs [14]) and synthetic (e.g., the intentional inactivation [4]) SM degradation effects by a general damping term.
- For the first time, we present a comprehensive theoretical characterization of different types of ISI, which only occur in closed-loop MC systems and were observed only experimentally before.
- Utilizing the proposed models, we analyze the impact of the different types of ISI occurring in closed-loop systems on long transmission sequences and investigate how localized degradation effects can mitigate ISI. In particular, we study how molecule degradation impacts whether or not the considered closed-loop system can be represented by an equivalent open-loop system.

The remainder of this paper is organized as follows. In Section 2, we introduce the considered closed-loop system model. In Section 3, we develop an analytical model and validate it with particle-based simulations (PBSs). In Section 4, we use the developed model to characterize different types of ISI. In Section 5, we present simulation results and Section 6 concludes the paper.

2 SYSTEM MODEL

As previously mentioned, in many future MC applications such as drug delivery or health monitoring, signals propagate along the CVS from a TX to an RX. Inside the CVS, SMs are transported mainly via advection and diffusion. Moreover, SMs may undergo degradation reactions, either gradually due to their irreversible absorption by vessel walls, e.g., in organs such as the liver, or intentionally, e.g., by inactivation².

The center of Fig. 1 shows a schematic of the CVS as a highly complex closed-loop system. Modeling the CVS in its full three-dimensional (3-D) geometry is very complex due to its intricate vascular network and the closed-loop topology. Therefore, we mimic the closed-loop characteristic of the CVS by a 3-D closed-loop pipe of constant radius r_0 and loop length L , i.e., a circumferential distance around the loop of length L . In this closed-loop pipe, SMs are transported by diffusion and laminar flow, and are affected by global or localized degradation reactions. Moreover, for high vascularization and due to the various phenomena affecting particle

²Additionally, reversible boundary interactions, such as the adsorption and desorption of SMs at the vessel wall, may play a role as well. This topic will be investigated in future work.

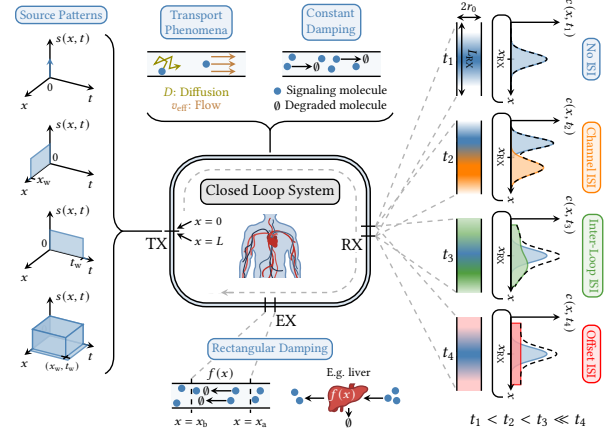


Figure 1: Schematic of the CVS and the mimicking of its closed-loop characteristic as a one-dimensional (1-D) closed-loop system (center). SMs are transported mainly by diffusion and flow and are affected by global (e.g., SM degradation) and spatially localized (e.g., SM absorption into organs) degradation, modeled as constant and rectangular damping (top and bottom). At TX, SMs can be injected with arbitrary temporal and spatial dynamics, modeled by the source term $s(x, t)$ (left). The different types of ISI occurring in closed-loop systems are shown on the right hand side.

propagation, it has been shown in [14] that the molecule transport in vascular networks is highly dispersive. Therefore, we assume that the SM transport between the TX and a transparent RX occurs in the dispersive regime [9], and we further simplify the 3-D closed-loop system to a 1-D closed-loop pipe. To this end, the SM concentration $c(x, t)$ over time t and space x in the closed-loop pipe is governed by the following 1-D advection-diffusion-reaction equation

$$\partial_t c(x, t) = D_{\text{eff}} \partial_x^2 c(x, t) - v_{\text{eff}} \partial_x c(x, t) - f(x) c(x, t) + s(x, t), \quad (1)$$

where ∂_t , ∂_x , and ∂_x^2 denote the first order partial derivative with respect to time t and the first- and second-order partial derivatives with respect to space x , respectively. Parameters D_{eff} in $\text{m}^2 \text{s}^{-1}$ and v_{eff} in m s^{-1} denote the effective diffusion coefficient of the SMs and the effective velocity of the fluid, respectively. The effective diffusion coefficient is given by $D_{\text{eff}} = D \left(1 + \frac{1}{48} \left(\frac{r_0 v_{\text{eff}}}{D} \right)^2 \right)$ [20, Eq. (12)], where D is the diffusion coefficient in the respective 3-D pipe of radius r_0 . The terms $f(x)$ and $s(x, t)$ in (1) are the spatially varying degradation function and the source term modeling SM injection, respectively. In the following sections, the term $f(x)$ is used to model different types of localized and global effects affecting the SMs such as intentional or non-intentional degradation and absorption of SMs in specific parts of the system. As all of these effects have in common that they lead to fewer received molecules at the RX, we refer to $f(x)$ as a damping term of $c(x, t)$. To account for the closed-loop system, (1) is defined on spatial domain $x \in [0, L]$, with periodic boundary conditions $\partial_x^k c(0, t) = \partial_x^k c(L, t)$, $\forall t \in \mathbb{R}^+$, $\forall k \in \mathbb{N}$, and initial condition $c(x, 0) = 0$, where \mathbb{R}^+ and \mathbb{N} denote the set of non-negative real numbers and the set of natural numbers, respectively.

3 SYSTEM RESPONSE

In this section, we propose an analytical model for SM propagation in closed-loop systems by solving the partial differential equation (PDE) in (1). Due to the periodicity of the spatial domain, concentration $c(x, t)$ in (1) can be expressed in terms of a Fourier series as

$$c(x, t) = \lim_{N \rightarrow \infty} \sum_{n=-N}^N \hat{c}_n(t) e^{jk_n x}, \quad (2)$$

with Fourier coefficients $\hat{c}_n(t)$ and Fourier basis functions $e^{jk_n x}$. Here, $k_n \in \mathbb{R}$ and j denotes the imaginary unit. We note that, for an exact solution, the number of terms in the sum in (2) needs to be infinity, i.e., $N \rightarrow \infty$. However, for mathematical tractability, in the following, we consider N to be finite and large enough to well approximate $c(x, t)$, which we validate with PBSs, cf. Section 3.4.

The periodic boundary condition requires for the basis functions $e^{jk_n L} = 1$, yielding wavenumbers $k_n = \frac{2\pi n}{L}$, $n \in \mathbb{Z}$. Similarly, the degradation function $f(x)$ and the source term $s(x, t)$ in (1) can be expanded into Fourier series as follows

$$\begin{aligned} f(x) &= \sum_{m=-N}^N \hat{f}_m e^{jk_m x}, \quad s(x, t) = \sum_{n=-N}^N \hat{s}_n(t) e^{jk_n x}, \quad (3) \\ \hat{f}_m &= \frac{1}{L} \int_0^L f(x) e^{-jk_m x} dx, \quad \hat{s}_n(t) = \frac{1}{L} \int_0^L s(x, t) e^{-jk_n x} dx, \end{aligned} \quad (4)$$

where \hat{f}_m and $\hat{s}_n(t)$ are the Fourier coefficients for the expansion of $f(x)$ and $s(x, t)$, respectively. Substituting (2) and (3) into (1) yields the following system of ordinary differential equations (ODEs) for the $2N + 1$ Fourier coefficients $\hat{c}_n(t)$:

$$\partial_t \hat{c}_n(t) = -D_{\text{eff}} k_n^2 \hat{c}_n(t) - v_{\text{eff}} j k_n \hat{c}_n(t) - \sum_{m=-N}^N \hat{f}_{n-m} \hat{c}_m(t) + \hat{s}_n(t). \quad (5)$$

3.1 Solution in Form of Matrix Exponential

To solve the system of ODEs in (5), we first define a $(2N + 1) \times 1$ vector of Fourier coefficients $\hat{\mathbf{c}}(t) = [\hat{c}_{-N}(t), \dots, \hat{c}_0(t), \dots, \hat{c}_N(t)]^\top$, where $[\cdot]^\top$ denotes transposition. Then, the system in (5) can be rewritten as

$$\partial_t \hat{\mathbf{c}}(t) = \mathbf{A} \hat{\mathbf{c}}(t) + \hat{\mathbf{s}}(t), \quad (6)$$

where \mathbf{A} is a $(2N + 1) \times (2N + 1)$ matrix and $\hat{\mathbf{s}}(t) = [\hat{s}_{-N}(t), \dots, \hat{s}_N(t)]^\top$ is the vector of coefficients $\hat{s}_n(t)$. The individual entries of matrix \mathbf{A} , $A_{n,m}$, are obtained by reformulating the system of ODEs in (5) into vector form as follows

$$A_{n,m} = \begin{cases} -D_{\text{eff}} k_n^2 - v_{\text{eff}} j k_n - \hat{f}_0 & \text{if } n = m, \\ -\hat{f}_{n-m} & \text{if } n \neq m. \end{cases} \quad (7)$$

The initial conditions for $\hat{\mathbf{c}}(t)$ at $t = 0$ in (6) follow from the initial condition $c(x, 0) = 0$ for PDE (1) as $\hat{\mathbf{c}}(0) = \mathbf{0}$, where $\mathbf{0} = [0, \dots, 0]^\top$ is a vector of zeros of length $(2N + 1) \times 1$. Inserting $\hat{\mathbf{c}}(0) = \mathbf{0}$ into (6), a solution for $\hat{\mathbf{c}}(t)$ can be obtained in terms of a matrix exponential as follows

$$\hat{\mathbf{c}}(t) = \int_0^t e^{\mathbf{A}(t-\tau)} \hat{\mathbf{s}}(\tau) d\tau. \quad (8)$$

Inserting (8) into Fourier series (2), the concentration $c(x, t)$ can be expressed as

$$c(x, t) = \mathbf{e}^\top(x) \hat{\mathbf{c}}(t) = \mathbf{e}^\top(x) \int_0^t e^{\mathbf{A}(t-\tau)} \hat{\mathbf{s}}(\tau) d\tau, \quad (9)$$

where the sum in (2) is reformulated into a matrix vector multiplication using the $(2N + 1) \times 1$ vector $\mathbf{e}(x) = [e^{jk_{-N}x}, \dots, e^{jk_Nx}]^\top$ of Fourier basis functions.

3.2 Global and Localized Damping

The function $f(x)$ captures global and spatially localized degradation mechanisms such as a constant baseline degradation (e.g., spontaneous switching of *green fluorescent protein variant "Dreiklang"* (GFPD), a variant of green fluorescent protein (GFP) [3], if used as SMs), and the localized clearance of SM (e.g., Indocyanine green (ICG) clearance from the vascular system and accumulation in an organ, e.g., the liver [18]). In the following, we first introduce a two-level damping function to model these effects, and then discuss several special cases.

3.2.1 Two-Level Damping. To model spatially varying damping effects, we define $f(x)$ as a function with two distinct levels, representing a spatially localized region of higher damping within a global degradation environment³

$$f(x) = \begin{cases} \alpha & \text{if } x \in [x_a, x_b], \\ \beta & \text{else,} \end{cases} \quad (10)$$

where $[x_a, x_b]$ indicates the spatial interval with higher damping constant $\alpha \geq \beta$ in s^{-1} , $0 \leq x_a < x_b \leq L$, and β in s^{-1} reflects the baseline degradation rate. In order to obtain a solution for concentration $c(x, t)$ in (1), the entries of matrix \mathbf{A} in (7) need to be derived. Inserting (10) into (4) the Fourier coefficients \hat{f}_m can be obtained as

$$\begin{aligned} \hat{f}_m &= \frac{1}{L} \left(\int_0^{x_a} \beta e^{-jk_m x} dx + \int_{x_a}^{x_b} \alpha e^{-jk_m x} dx + \int_{x_b}^L \beta e^{-jk_m x} dx \right) \\ &= \begin{cases} \beta + \frac{(\alpha - \beta)(x_b - x_a)}{L} & \text{if } m = 0, \\ \frac{(\alpha - \beta)}{\pi m} e^{-\frac{jk_m(x_a + x_b)}{2}} \sin\left(\frac{k_m(x_b - x_a)}{2}\right) & \text{if } m \neq 0. \end{cases} \end{aligned} \quad (11)$$

Inserting (11) into (7), the entries $A_{n,m}$ of the matrix \mathbf{A} follow as

$$A_{n,m} = \begin{cases} -D_{\text{eff}} k_n^2 - v_{\text{eff}} j k_n - \beta - \frac{(\alpha - \beta)(x_b - x_a)}{L} & \text{if } n = m, \\ -\frac{(\alpha - \beta)}{\pi(n-m)} e^{-\frac{jk_{n-m}(x_a + x_b)}{2}} \sin\left(\frac{k_{n-m}(x_b - x_a)}{2}\right) & \text{if } n \neq m. \end{cases} \quad (12)$$

Inserting matrix \mathbf{A} with the entries in (12) into (9) yields an analytical solution for the SM concentration in a 1-D closed-loop system accounting for the combined effects of diffusion, advection, and spatially varying damping.

3.2.2 Special Cases of Damping. The general solution for the entries of matrix \mathbf{A} in (12) accounts for both global and localized damping effects simultaneously. By varying parameters α and β in (10), different special cases can be modeled, for which the entries $A_{n,m}$ simplify.

For *localized damping*, $\beta = 0$, i.e., damping occurs only within $[x_a, x_b]$ with rate $\alpha > 0$. This models scenarios, where damping

³For simplicity, we consider a single high-damping region, but $f(x)$ can be readily extended to multiple regions with varying damping.

is confined to a specific region, such as the absorption of SMs by organs, with negligible loss elsewhere.

For *global damping*, $\alpha = \beta > 0$, resulting in $f(x) = \beta$ across the entire spatial domain. This represents a system with homogeneous degradation, which models, e.g., a constant enzymatic degradation of SMs everywhere.

For *no damping*, $\alpha = \beta = 0$, so $f(x) = 0$, modeling a system without degradation or damping effects. This simplifies (1) to an advection-diffusion equation with known solutions [14, Eq. (3)].

3.3 Forms of Signaling Molecule Release

In general, the function $s(x, t)$ can model any spatio-temporal release pattern of SMs. In the following, we derive the source term Fourier coefficients $\hat{s}(t)$ needed for the solution in (9) for two specific cases. The first case is an instantaneous release of SMs at a single point in space. The second case is a spatially extended distribution of SMs that is released instantaneously.

3.3.1 SM Point Release. For an instantaneous release of N_p SMs at $x = 0$ and $t = 0$, the source function and its Fourier coefficient vector (obtained by inserting the source function into (4)) are given as

$$s(x, t) = N_p \delta(x) \delta(t), \quad \hat{s}(t) = \frac{N_p}{L} \delta(t) \mathbf{1}, \quad (13)$$

where $\mathbf{1} = [1, \dots, 1]^T$.

Substituting $\hat{s}(t)$ into (9), $c(x, t)$ follows as

$$c(x, t) = \frac{N_p}{L} \mathbf{e}^T(x) \mathbf{e}^{At} \mathbf{1}. \quad (14)$$

3.3.2 Spatially Distributed SM Release. Considering N_p SMs released instantaneously at $t = 0$ spatially over $[0, x_w]$, with $x_w < L$, the source function follows as

$$s(x, t) = N_p \frac{\mathbb{1}_{[0, x_w]}(x)}{x_w} \delta(t), \quad (15)$$

with indicator function $\mathbb{1}_{[0, x_w]}(x) = 1$ for $0 \leq x \leq x_w$, and 0 otherwise. Inserting (15) into (4) yields the source term's Fourier coefficients as

$$\hat{s}_n(t) = \frac{N_p}{L} \int_0^L \delta(t) \frac{\mathbb{1}_{[0, x_w]}(x)}{x_w} e^{-jk_n x} dx = \frac{N_p}{L} \frac{\delta(t)}{x_w} \int_0^{x_w} e^{-jk_n x} dx, \quad (16)$$

and the source's Fourier coefficient vector $\hat{s}(t)$ follows as

$$\hat{s}(t) = \frac{N_p}{L} \delta(t) \boldsymbol{\phi}, \quad \phi_n = \begin{cases} \frac{1}{x_w} \frac{1 - e^{-jk_n x_w}}{jk_n} & n \neq 0, \\ 1 & n = 0, \end{cases} \quad (17)$$

where $\boldsymbol{\phi} = [\phi_{-N}, \dots, \phi_N]^T$. Inserting (17) in (9), $c(x, t)$ for a spatially distributed release of SMs can be obtained as follows

$$c(x, t) = \mathbf{e}^T(x) \hat{c}(t) = \frac{N_p}{L} \mathbf{e}^T(x) \mathbf{e}^{At} \boldsymbol{\phi}. \quad (18)$$

3.4 Comparison Between Analytical Solution and Particle-Based Simulation

With the PBSs, we validate the accuracy of the simplification step of reducing the model of the 3-D pipe to a 1-D model. Additionally, we validate that for $N = 100$, i.e., when the Fourier series in (2) is truncated to $2N + 1 = 201$ terms, $c(x, t)$ is well approximated.

In particular, we validate the analytical solution in (9) for an instantaneous point-release of SMs, cf. (13), and a system comprising two levels of damping, cf. (10). For generality, we consider the four scenarios depicted in Fig. 2, with two different damping constants

α and two different positions of the transparent RX and damping region $[x_a, x_b]$, respectively. The values of α and the limits of the RX and the damping region are shown in Fig. 2. Outside the localized damping region, i.e., outside the interval $[x_a, x_b]$, a constant damping of $\beta = 0.01 \text{ s}^{-1}$ is considered. The default values of all system parameters are given in Table 1 and are used throughout the paper, if not specified otherwise.

The analytical results in this section are based on (14), i.e., a point release. The received concentration follows as $c_{RX}(t) = c(x_{RX}, t)$, i.e., by sampling $c(x, t)$ at axial position $x = x_{RX}$. For RXs of spatial extent (as the ones in Fig. 2), the received concentration $c_{RX}(t)$ is obtained by integrating (14) over the spatial interval $[x_{RX,a}, x_{RX,b}]$

$$c_{RX}(t) = \int_{x_{RX,a}}^{x_{RX,b}} c(x, t) dx, \quad (19)$$

where $[x_{RX,a}, x_{RX,b}]$ with $0 \leq x_{RX,a} < x_{RX,b} \leq L$ denote the limits of the RX region. For the latter, the center position of the RX is given by $x_{RX} = (x_{RX,a} + x_{RX,b})/2$.

3.4.1 Details of the Particle-Based Simulation. The PBSs are performed for a 3-D straight pipe of length L with *reflective radial boundaries* and *periodic boundaries* at $x = 0$ and $x = L$. At time $t = 0$, N_p particles are uniformly distributed over the cross section of the pipe at $x = 0$. For $t > 0$, the particles in the pipe are propagated by diffusion and laminar flow in x direction with a parabolic flow profile, i.e., $v_x(r_p) = 2v_{\text{eff}} \left(1 - (r_p/r_0)^2\right)$. Here, v_x and r_p are the particle's velocity in x direction induced by flow and the distance of the particle from the x axis, i.e., the centerline of the 3-D pipe, respectively. The clearance of the SMs is realized as a first-order degradation reaction, implemented by the stochastic simulation algorithm (SSA) [6]. All results shown are normalized by N_p .

Table 1: Parameters used in the PBS and analytical solution.

Parameter	Description	Value	Unit
D_{eff}	Effective diffusion coefficient	5×10^{-3}	$\text{m}^2 \text{s}^{-1}$
L	Length	6	m
r_0	Radius of pipe	0.02	m
v_{eff}	Effective velocity	0.1	m s^{-1}
α	Degradation rate in $[x_a, x_b]$	$\{0.05, 0.1\}$	s^{-1}
β	Degradation rate outside $[x_a, x_b]$	0.01	s^{-1}
N_p	Number of particles	10,000	–
Δt	PBS time step	10^{-6}	s
T	Total simulation time	100	s

3.4.2 Model Verification. Figure 3 shows the analytical and PBS results for all four scenarios summarized in Fig. 2. We observe that the results obtained from PBS (solid lines) and the proposed analytical solution (shaded lines) are in excellent agreement, confirming the accuracy of the derived model. Moreover, the effects introduced by the closed-loop system (repeated observation of the same SMs) and the different types of damping can be observed. First, we observe that the received signal amplitude is damped over time, where the damping is more pronounced for Scenarios 1 and 3, cf. Fig. 2, as rate α is higher in these cases, thus yielding, as expected, a stronger damping. For Scenarios 1 and 2, cf. Fig. 2, where the RX is located between the TX and the damping region, the first observed peak is

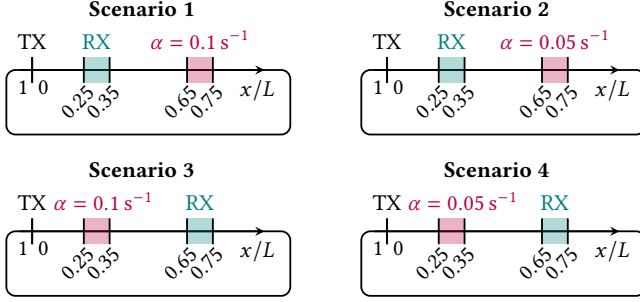


Figure 2: 1-D representation of four different closed-loop scenarios considered for verification of the proposed model.

affected by the global damping only, while subsequent peaks are attenuated by the effects of local damping constant α and global damping constant β . This observation suggests that damping at a properly chosen location and with a suitable rate α can mitigate ISI in an MC system without large effects on the first peak of the transmission (see Section 4). In comparison, in Scenarios 3 and 4, cf. Fig. 2, where the RX is placed behind the damping region, already the first peak observed at the RX is damped significantly.

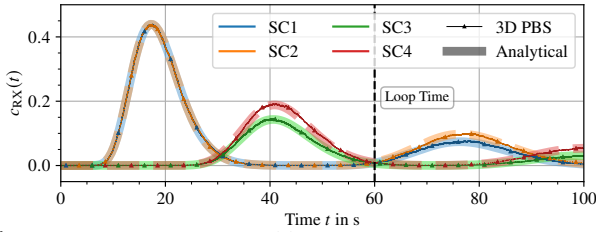


Figure 3: Received signal $c_{RX}(t)$ obtained with the analytical solution (14) (shaded lines) and by PBS (solid lines). The different colors indicate the different scenarios shown in Fig. 2.

4 COMMUNICATION SYSTEM AND ANALYSIS

In this section, we use the analytical model for the SM concentration, $c(x, t)$, obtained in Section 3, to investigate the impact of a closed-loop system with constant and/or localized damping on MC-based information transmission. In the following, we consider a closed-loop MC system employing ON-OFF keying (OOK) modulation. In this setup, the TX releases N_p signaling molecules for the transmission of bit 1 and does not release any molecules for bit 0. The binary bit sequence can be represented by an impulse train as follows

$$b(t) = \sum_{p=0}^{B-1} \tilde{b}_p \delta(t - pT_S - t_0), \quad (20)$$

where B , \tilde{b}_p , T_S , and t_0 denote the total number of transmitted bits, i.e., the sequence length, the p -th transmitted bit with $p \in \{0, 1, \dots, B-1\}$ and $\tilde{b}_p = 1$ for bit 1 and $\tilde{b}_p = 0$ for bit 0, the symbol interval duration, and the transmission start time, respectively. Upon release of the binary sequence in (20) by the TX, the received signal $r(t)$ at the RX results from the linear superposition of the individual system responses $c(x, t)$, cf. (18), caused by different symbols. Consequently, the received signal $r(t)$ is obtained by convolving $c_{RX}(t)$ with $b(t)$ as follows

$$r(t) = b(t) * c_{RX}(t), \quad (21)$$

where $*$ denotes the convolution operator. For simplicity, all results for $r(t)$ presented in Section 5 are normalized by N_p . Additionally, we assume that $\tilde{b}_p = 1$ and $\tilde{b}_p = 0$ occur equally often in the binary sequence. In the next section, the signal $c(x, t)$ is used to classify different types of ISI, before the analysis is extended to the received signal $r(t)$ in Section 5.

4.1 Inter-Symbol Interference

A key challenge in MC is the occurrence of ISI. Specifically, the modulated signal can overlap with signals from previous and subsequent symbol intervals, leading to causal and anticausal ISI [19] at the RX, cf. Fig. 1. In most advection-diffusion-based MC systems considered so far, any released SM appears only once at the RX. However, in closed-loop systems, SMs persist as they circulate repeatedly inside the system, causing ISI multiple times. In other words, a closed-loop system represents a multi-path propagation environment as each circulation loop delivers the SMs to the RX again, while only the first arrival contains the desired⁴ information. While the length of the direct path is given by the distance between TX and RX, each subsequent path is elongated by the loop length L . As a result, these 'looped' versions of the signal arrive as different dispersed versions of the original signal at staggered times at the RX, interfering with both neighboring symbols and those transmitted much later.

The resulting unique types of ISI in closed-loop systems, introduced as *inter-loop* ISI and *offset* ISI in [16], require targeted mitigation strategies, such as customized localized SM clearance blocks or tailor-made equalization techniques. Developing such strategies is crucial, yet challenging, as these types of ISI have not been quantitatively characterized to date. Therefore, before mitigation strategies can be developed, it is imperative to provide a clear mathematical definition and characterization of each type of ISI occurring in closed-loop systems. Assuming that TX and RX in a closed-loop MC system are positioned such that the first and highest peak of the received signal is due to SMs propagating in the direction of the flow, the time of arrival of the first peak at the RX is given by [20, Eq. (14)]

$$t_p = t_0 + \frac{-D_{\text{eff}} + \sqrt{D_{\text{eff}}^2 + (x_{\text{RX}} - x_{\text{TX}})^2 v_{\text{eff}}^2}}{v_{\text{eff}}^2}, \quad (22)$$

where $x_{\text{TX}} = x_w/2$ for spatial distributed SM release (see Section 3.3.2)⁵. In the following, we discuss the different types of ISI occurring in closed-loop systems in more detail.

4.1.1 Channel ISI. Channel ISI arises due to the overlap of SMs from neighboring symbol intervals during the propagation from TX to RX, and has been extensively studied in the MC literature [13]. Specifically, channel ISI is caused by SMs arriving at the RX outside of their designated symbol interval of duration T_S centered around the peak arrival time t_p , without having yet completed a full circulation in the closed-loop system.

⁴Of course, this statement only holds when symbol-by-symbol detection is used.

⁵We note that for special cases, such as diffusion-dominated propagation of SMs against the flow direction, the peak time t_p in (22), which assumes downstream communication, is not valid. However, as such scenarios are considered to have limited practical relevance, they are not addressed in this work.

To obtain a mathematical description for the channel ISI in closed-loop systems, only the contribution of those SMs that cause interference on their direct path from TX to RX should be included. The contribution of the direct path $c_{\text{RX}}^{\text{open}}(t)$ to the received signal $c_{\text{RX}}(t)$ can be obtained either by solving the corresponding open-loop system, i.e., by considering (1) without periodic boundary conditions, as shown for a closed-loop system without damping in [14, Fig. 8] or by taking the limit value for $L \rightarrow \infty$ of the closed-loop model solution in (9) derived in this work. Hence, the concentration component $c_c(t)$ attributable to channel ISI can be defined as

$$c_c(t) = \begin{cases} c_{\text{RX}}^{\text{open}}(t) & \forall t \in \left[t_0, \max(t_0, t_p - \frac{T_s}{2}) \right) \cup \left[t_p + \frac{T_s}{2}, \infty \right) \\ 0 & \text{else} \end{cases}, \quad (23)$$

The desired signal component $c_d(t)$ follows as

$$c_d(t) = \begin{cases} c_{\text{RX}}^{\text{open}}(t) & \forall t \in \left[\max(t_0, t_p - \frac{T_s}{2}), t_p + \frac{T_s}{2} \right) \\ 0 & \text{else} \end{cases}, \quad (24)$$

i.e., the signal centered around t_p .

4.1.2 Inter-Loop ISI. The second type of ISI in closed-loop systems is *inter-loop ISI*. It emerges due to the recirculation of SMs in the system, i.e., after completion of at least one circulation, SMs reappear at the RX as peaks (cf. Fig. 3) and possibly interfere with SMs from subsequent symbol intervals. To mathematically quantify inter-loop ISI, we can subtract the open-loop solution $c_{\text{RX}}^{\text{open}}(t)$ (representing the contribution from the direct path) from the total concentration observed in the closed-loop system $c_{\text{RX}}(t)$ as follows

$$c_i(t) = \begin{cases} c_{\text{RX}}(t) - c_{\text{RX}}^{\text{open}}(t) & \forall t \in [t_0, t_i] \\ 0 & \text{else} \end{cases}, \quad (25)$$

where t_i denotes the time when inter-loop ISI transitions into a constant signal, which we refer to as an offset. This time can be identified based on the fraction of the global signal decay, described by the 0th mode of the respective solution, and the received signal as follows

$$t_i := \inf \left\{ t \in \mathbb{R}_{\geq 0} \mid \forall \tau \geq t : \left| \frac{\hat{c}_0(\tau) - \hat{c}_0^{\text{open}}(\tau)}{c_{\text{RX}}(\tau) - c_{\text{RX}}^{\text{open}}(\tau)} \right| \geq \epsilon \right\}, \quad (26)$$

where $\hat{c}_0(t)$ denotes the $n = 0$ mode of $c(x, t)$ in (9), similarly $\hat{c}_0^{\text{open}}(t)$ denotes the 0th mode of the corresponding open-loop solution. Therefore, (26) ensures that as soon as the zero-frequency component, i.e., the offset component (numerator in (26)), exceeds a threshold fraction ϵ of the total received inter-loop ISI signal (denominator in (26)), the received signal is considered as offset ISI, which is explained next.

4.1.3 Offset ISI. The third type of ISI occurring in closed-loop systems is *offset ISI*. It represents the persistent shift in signal baseline caused by the accumulation of SMs circulating in the system. As SMs disperse during circulation, their influence on the signal received at the RX transitions from discrete interferences, denoted as inter-loop ISI, to a continuous offset in the received signal. The offset ISI part of the signal can be defined as follows

$$c_o(t) = \begin{cases} c_{\text{RX}}(t) - c_{\text{RX}}^{\text{open}}(t) & \forall t > t_i \\ 0 & \text{else} \end{cases}. \quad (27)$$

4.2 Closed-Loop Equilibrium Concentration

As an additional quantity for the characterization of closed-loop systems, we define an equilibrium concentration of SMs in the system, r_{eq} , as the concentration where, on average per symbol interval, the number of SMs removed from the system due to damping equals the number of SMs released into the system, as follows

$$\underbrace{N_p/2}_{\text{average release per symbol}} = \underbrace{r_{\text{eq}} T_s ((x_b - x_a)\alpha + (L - (x_b - x_a))\beta)}_{\text{average damping per symbol}} \\ \rightarrow r_{\text{eq}} = \frac{N_p}{2T_s ((x_b - x_a)\alpha + (L - (x_b - x_a))\beta)}. \quad (28)$$

This equilibrium concentration inherently captures the accumulation of SMs within the closed-loop system after repeated SM injections. This provides an estimate of the operational concentration range of SMs over extended transmission times.

5 EVALUATION

In this section, we analyze the various types of ISI occurring in closed-loop systems for long transmission sequences and investigate the effect of localized damping on the received signal.

5.1 Temporal Evolution of ISI During Continuous Transmission

First, we investigate the emergence and progression of the different types of ISI during continuous information transmission. To analyze the system behavior, we apply the formal definitions of the different types of ISI from Section 4 on a symbol-by-symbol basis and compute the received signal $r(t)$ by convolving the input sequence with the system response, see (21). As evaluation scenario, we consider Scenario 1, as depicted in Fig. 2.

In this scenario, the TX transmits a binary sequence $b(t)$, as defined in (20), of length $B = 300$ bits. As symbol duration, $T_s = 5$ s is used. The corresponding received signal $r(t)$ (solid black line) along with its constituent components is presented in Fig. 4. Specifically, $r(t)$ consists of the desired signal $r_d(t)$ (blue), channel ISI $r_c(t)$ (orange), inter-loop ISI $r_i(t)$ (green), and offset ISI $r_o(t)$ (red). For reference, the contribution of the first transmitted bit 1 is shown separately as $c_{\text{RX}}(t)$ (dashed brown line in the upper-left inset), along with the received signal of a corresponding open-loop system, $r^{\text{open}}(t)$, and the system's equilibrium concentration, r_{eq} (horizontal dotted line), cf. (28).

From the insets in Fig. 4, we observe that $r(t)$ increases for the transmission of bit 1s. The upper left shows that during the first 9 bits, $r(t)$ comprises only the desired signal and channel ISI, as no SMs have yet completed a full loop through the system. The emergence of the second peak from the first bit 1, after one circulation, shown in the upper-left inset, marks the onset of inter-loop ISI. Thereafter, inter-loop ISI is progressively increasing, as the cumulative contributions of SMs completing one or more full loops increases. At around $t = 450$ s, the contribution from the first transmitted bit becomes sufficiently damped to satisfy the criteria for offset ISI, cf. (26) and (27), which thereafter increases, before it saturates at around $t = 1300$ s.

Towards the end of the transmission sequence, we observe from Fig. 4 that $r(t)$ approaches the equilibrium concentration r_{eq} . We note that in this phase of the transmission, the peak amplitude of

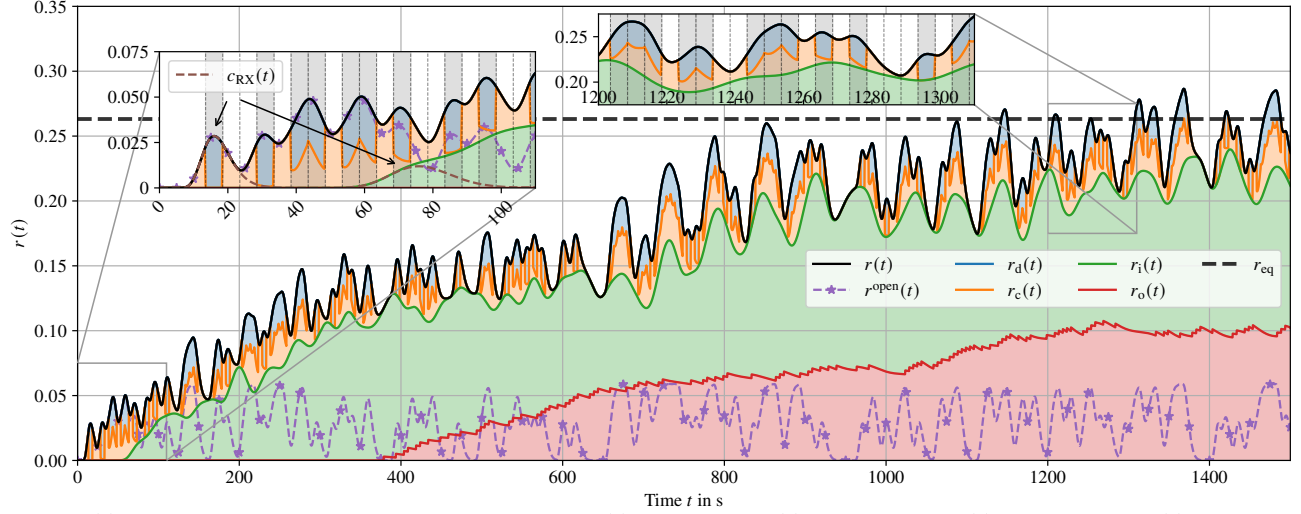


Figure 4: $r(t)$ is decomposed into the desired received signal $r_d(t)$, channel ISI $r_c(t)$, inter-loop ISI $r_i(t)$, and offset ISI $r_o(t)$. Additionally, $r^{\text{open}}(t)$ and the received signal due to the first transmitted bit 1 ($c_{\text{RX}}(t)$), shown in the upper-left inset) are provided. Here, $x_{\text{RX}} = 0.3L$, $N = 1000$, $\epsilon = 0.8$, $\alpha = 0.01 \text{ s}^{-1}$, $\beta = 0.001 \text{ s}^{-1}$, and a rectangular TX with $x_w = 0.3 \text{ m}$, cf. Section 3.3.2, are used. The shaded areas in the insets indicate the transmission of bit 1.

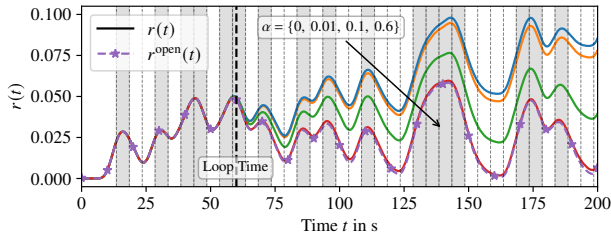


Figure 5: Evaluation of the evolution of $r(t)$ for different localized damping constants $\alpha = \{0, 0.01, 0.1, 0.6\} \text{ s}^{-1}$. Additionally, for comparison, $r^{\text{open}}(t)$ is shown. Here, $x_{\text{RX}} = 0.3L$, $N = 250$, $\beta = 0.001 \text{ s}^{-1}$, and a rectangular TX with $x_w = 0.3 \text{ m}$, cf. Section 3.3.2, are used. Shaded areas correspond to the transmission of bit 1.

individual bit-1 transmissions received at the RX is approximately 0.025, which is nearly one order of magnitude below $r_{\text{eq}} = 0.26$. Given this ratio of 0.025 from SMs compared to 0.26 from residual molecules originating from previous transmissions, reliable communication is expected to become increasingly challenging, if not impossible. Note that, while we show the concentration here, i.e., the expected received signal, the actual received signal will be noisy due to diffusion and receiver noise and the desired signal $r_d(t)$ may be completely obscured.

These observations highlight the importance of understanding the distinct ISI components and the role of the equilibrium concentration r_{eq} when analyzing or designing MC systems for long-term operation in closed-loop environments. Specifically, systems with high r_{eq} values compared to the desired signal amplitudes require effective ISI mitigation strategies to enhance communication reliability. One such strategy involves increased localized damping to suppress the endless circulation of SMs, as explored in the following section.

5.2 Effect of Localized Damping on Emulating Open-Loop Behavior

In Fig. 5, we investigate the influence of localized damping on the received signal $r(t)$. In particular, we consider the setup from Scenario 1 in Fig. 2, and vary the damping constant from $\alpha = 0 \text{ s}^{-1}$ (blue) to $\alpha = 0.6 \text{ s}^{-1}$ (red). For comparison, Fig. 5 also includes the received signal $r^{\text{open}}(t)$ (dotted) of the corresponding open-loop system.

From Fig. 5, we observe that until $t = 60 \text{ s}$ the received signals $r(t)$ for all considered damping constant α coincide, as the damping region is positioned downstream of the RX (see Fig. 2). Consequently, the damping only affects SMs revisiting the RX after one circulation. Therefore, in the considered arrangement, the damping only affects, and could possibly mitigate, inter-loop and offset ISI, but not channel ISI. As shown in Fig. 5, the received signal $r(t)$ is attenuated to different degrees depending on the value of α . This occurs because the portion of the signal originating from SMs that have completed at least one cycle is attenuated. Moreover, Fig. 5 shows that when α is sufficiently high (e.g., $\alpha = 0.6 \text{ s}^{-1}$), the received signal $r(t)$ closely matches the corresponding open-loop system's $r^{\text{open}}(t)$. This suggests that the effects of interference caused by the specific properties of closed-loop systems can be mitigated by localized damping. This finding is particularly important for designing practical MC systems, as it may allow closed-loop systems to operate in a regime where analytical tools and models already developed for open-loop MC systems can be applied directly.

6 CONCLUSION

In this paper, a novel physics-based model for the propagation of molecular signals in closed-loop MC systems was proposed along with a reformulation of the system's descriptive equations that allows for efficient numerical evaluation. The model encompasses arbitrary spatio-temporal molecule release profiles and can represent different types of molecule degradation that are practically

relevant for natural and synthetic SM degradation/clearance. The presented results allow, for the first time, to rigorously distinguish different types of ISI that can occur in closed-loop MC systems. Furthermore, they reveal under which conditions the open loop assumption made in many MC models is an accurate approximation of a closed-loop system.

Extending the model proposed in this paper to branched vessel topologies can be an interesting topic for future research.

REFERENCES

- [1] Ian F. Akyildiz, Massimiliano Pierobon, and Sasitharan Balasubramaniam. 2019. Moving forward with molecular communication: From theory to human health applications [point of view]. *Proc. IEEE* 107, 5 (May 2019), 858–865.
- [2] Ian F. Akyildiz, Max Pierobon, Sasi Balasubramaniam, and Y. Koucheryavy. 2015. The Internet of Bio-Nano Things. *IEEE Commun. Mag.* 53, 3 (March 2015), 32–40.
- [3] Tanja Brakemann, Andre C. Stiel, Gert Weber, Martin Andresen, Ilaria Testa, Tim Grotjohann, Marcel Leutenegger, Uwe Plessmann, Henning Urlaub, Christian Eggeling, et al. 2011. A reversibly photoswitchable GFP-like protein with fluorescence excitation decoupled from switching. *Nat. Biotechnol.* 29, 10 (Sept. 2011), 942–947.
- [4] Lukas Brand, Maike Scherer, Teena tom Dieck, Sebastian Lotter, Maximilian Schäfer, Andreas Burkovski, Heinrich Sticht, Kathrin Castiglione, and Robert Schober. 2024. Closed Loop Molecular Communication Testbed: Setup, Interference Analysis, and Experimental Results. In *Proc. IEEE Int. Conf. Commun.* 4805–4811.
- [5] Youssef Chahibi, Massimiliano Pierobon, Sang Ok Song, and Ian F. Akyildiz. 2013. A Molecular Communication System Model for Particulate Drug Delivery Systems. *IEEE Trans. Biomed. Eng.* 60, 12 (June 2013), 3468–3483.
- [6] Radek Erban and S. Jonathan Chapman. 2020. *Stochastic Modelling of Reaction-Diffusion Processes*. Cambridge University Press, Cambridge, U.K.
- [7] Jorge Torres Gómez, Regine Wendt, Anke Kuestner, Ketki Pitke, Lukas Stratmann, and Falko Dressler. 2021. Markov Model for the Flow of Nanobots in the Human Circulatory System. In *Proc. 8th Ann. ACM Int. Conf. Nanoscale Comp. Commun.* 1–7.
- [8] Timo Jakumeit, Lukas Brand, Jens Kirchner, Robert Schober, and Sebastian Lotter. 2025. Molecular Signal Reception in Complex Vessel Networks: The Role of the Network Topology. *Presented at IEEE Int. Conf. Commun.* (2025).
- [9] Vahid Jamali, Arman Ahmadzadeh, Wayan Wicke, Adam Noel, and Robert Schober. 2019. Channel modeling for diffusive molecular communication—A tutorial review. *Proc. IEEE* 107, 7 (July 2019), 1256–1301.
- [10] Ghazaleh Kianfar, Mehdi Azadi, Jamshid Abouei, Arash Mohammadi, and Konstantinos N. Plataniotis. 2024. Wireless Body Area Nanonetworks via Vascular Molecular Communication. *IEEE Trans. NanoBiosci.* 23, 2 (April 2024), 355–367.
- [11] Sebastian Lotter, Lukas Brand, Vahid Jamali, Maximilian Schäfer, Helene M. Loos, Harald Unterwiesing, Sandra Greiner, Jens Kirchner, Christoph Alexiou, Dietmar Drummer, Georg Fischer, Andrea Buettner, and Robert Schober. 2023. Experimental Research in Synthetic Molecular Communications – Part II. *IEEE Nanotechnol. Mag.* 17, 3 (June 2023), 54–65.
- [12] Reza Mosayebi, Arman Ahmadzadeh, Wayan Wicke, Vahid Jamali, Robert Schober, and Masoumeh Nasiri-Kenari. 2018. Early cancer detection in blood vessels using mobile nanosensors. *IEEE Trans. NanoBiosci.* 18, 2 (April 2018), 103–116.
- [13] Massimiliano Pierobon and Ian F. Akyildiz. 2012. Intersymbol and co-channel interference in diffusion-based molecular communication. In *Proc. IEEE Int. Conf. Commun.* 6126–6131.
- [14] Maximilian Schäfer, Andreas Ettner-Sitter, Lukas Brand, Sebastian Lotter, Fardad Vakiliipoor, Thiha Aung, Silke Haerteis, and Robert Schober. 2024. The Choroidal-lenticular Membrane Model: A 3D in vivo Testbed for Design and Analysis of MC Systems. In *Proc. 11th Ann. ACM Int. Conf. Nanoscale Comp. Commun.* 47–53.
- [15] Maximilian Schäfer, Wayan Wicke, Lukas Brand, Rudolf Rabenstein, and Robert Schober. 2021. Transfer function models for cylindrical MC channels with diffusion and laminar flow. *IEEE Trans. Mol. Biol. Multi-Scale Commun.* 7, 4 (Feb. 2021), 271–287.
- [16] Maike Scherer, Lukas Brand, Louis Wolf, Maximilian Schäfer, Sebastian Lotter, Andreas Burkovski, Heinrich Sticht, Robert Schober, Kathrin Castiglione, et al. 2025. Closed-Loop Long-Term Experimental Molecular Communication System. *arXiv version arXiv:2502.00831* (2025).
- [17] Nunzio Tuccitto, Giovanni Li-Destri, Grazia M. Messina, and Giovanni Marletta. 2017. Fluorescent quantum dots make feasible long-range transmission of molecular bits. *J. Phys. Chem. Lett.* 8, 16 (Aug. 2017), 3861–3866.
- [18] Fardad Vakiliipoor, Andreas Ettner-Sitter, Lukas Brand, Sebastian Lotter, Thiha Aung, Silke Haerteis, Robert Schober, and Maximilian Schäfer. 2025. The CAM Model: An in vivo Testbed for Molecular Communication Systems. *arXiv version arXiv:2504.12123* (2025).
- [19] Jiaming Wang, Dongyin Hu, Chirag Shetty, and Haitham Hassanieh. 2020. Understanding and embracing the complexities of the molecular communication channel in liquids. In *Proc. Annu. Int. Conf. Mobile Comput.* 1–15.
- [20] Wayan Wicke, Tobias Schwering, Arman Ahmadzadeh, Vahid Jamali, Adam Noel, and Robert Schober. 2018. Modeling duct flow for molecular communication. In *Proc. IEEE Global Commun. Conf.* 206–212.